RSC Advances

ROYAL SOCIETY OF CHEMISTRY

www.rsc.org/advances

Enhanced Thermoelectric Performance in Mg and Ca Substituted CdO Ceramics

Linjie Gao[a], Shufang Wang[a,*], Ran Liu[a], Xinyu Zha[a], Niefeng Sun[b], Shujie Wang[b], Jianglong Wang[a] and Guangsheng Fu[a,*]

[a] *Hebei Key Lab of Optic-electronic Information and Materials, The College of Physics Science and Technology, Hebei University, Baoding, 071002, China. Email: sfwang@hbu.edu.cn and fugs@hbu.edu.cn; Tel.: 86-312-5077370; Fax: 86-312-5077370*

[b] *National Key Laboratory of ASIC, Hebei Semiconductor Research Institute, Shijiazhuang, 050051, China*

Abstract

We report a more than 50% enhancement in the thermoelectric figure of merit *ZT* of CdO ceramics *via* simultaneous substituting with Mg and Ca. The Mg and Ca substitution is found to greatly suppress both the electrical and the lattice thermal conductivities of CdO while maintaining a moderate power factor. Detailed mechanisms are proposed to explain the experimental results. A *ZT* value of 0.5 at about 1000 K has been achieved in the optimum substituted sample, which is the highest *ZT* ever reported among the n-type oxide thermoelectric materials in this temperature range.

Keywords: CdO ceramics; Substitution; Thermal conductivity; *ZT*

1. Introduction

Thermoelectric (TE) conversion is an intriguing technology for the future sustainable society. In the past few decades, thermoelectric materials have been extensively studied and widely used in the fields of waste-heat power generation and Freon-free refrigeration [1-3]. The efficiency of TE materials is evaluated by the dimensionless figure of merit *ZT*, where three crucial parameters of Seebeck coefficient *S*, electrical resistivity ρ and thermal conductivity κ are concerned through the relation of $ZT=S^2T/\rho\kappa$.

Oxide thermoelectric materials are very promising in the high temperature region. In their short history of less than 20 years, the TE performances of oxides have been greatly improved [4-6]. Although the efficiencies of some p-type layered oxides are comparable with alloy TE materials [7-9], the *ZT* values of n-type oxides, such as $SrTiO_3$, $CaMnO_3$, ZnO and In_2O_3-based ceramics are still low[10-17]. Therefore, searching for new n-type oxides with good TE performance is crucial for the development of oxide TE devices.

CdO is a high mobility transparent conductive oxide that has been widely used in the field of optoelectronics. Recently, we found that CdO also exhibits good TE performance with the *ZT* value exceeds 0.3 at 1000 K [18-19], comparable to most n-type oxides. However, due to the simple cubic structure, the thermal conductivity of CdO is high (~8W/mK at about room temperature [20-21]), which lowers its TE efficiency and limits the interest in CdO for thermoelectric application. Here in this work, we report enhanced TE performances of n-type CdO-based thermoelectric ceramics *via*

suppressing the thermal conductivity by Ca and Mg substitution. Using this strategy, a *ZT* value of 0.5 is obtained at about 1000 K for the optimum sample, which is the highest value reported so far for the n-type oxide thermoelectric materials in this temperature range.

2. Experimental

The $Cd_{1-x-y}Mg_xCa_yO$ ($0 \leq x, y \leq 0.05$) ceramics were synthesized by a conventional solid-state reaction method. Commercial CdO (98.9%, Alfa Aesar, China), MgO (98%, Tianda Chemical Reagent, China) and CaO (99%, Tianjin Fuchen Chemical Reagents, China) powders were used as starting materials. Stoichiometric amounts of starting powders were weighed and wet milled for 12 h in a planetary mill, then the suspension was completely dried in an oven at 353 K for 6 h. After fully grinding, the dried powders were pelletized into pellets at room temperature, and then sintered in a muffle furnace. The typical sintering procedure started with a quick heating to 1173 K with the rate of 10 K/min, followed by holding at 1173 K for 20 h, and then a slow cooling with the rate of 1 K/min to 473 K before naturally cooled to room temperature. Finally, ceramic samples with nominal compositions of CdO, $Cd_{0.98}Mg_{0.01}Ca_{0.01}O$, $Cd_{0.96}Mg_{0.03}Ca_{0.01}O$, $Cd_{0.96}Mg_{0.01}Ca_{0.03}O$, $Cd_{0.94}Mg_{0.03}Ca_{0.03}O$ and $Cd_{0.90}Mg_{0.05}Ca_{0.05}O$ were obtained.

Phase identification and lattice parameter determination of the samples were conducted using X-ray diffraction (XRD, Bruker D8 Advance, Germany) with Cu Kα radiation at room temperature. Field-effect scanning electron microscopy (FESEM, FEI Nova Nano SEM 450, American) coupled with energy-dispersive X-ray (EDX)

detector were used to study the microstructures of the samples. The room temperature carrier concentration n and carrier mobility μ were measured using the Van Der Pauw method with an ET-9000 Hall effect measurement system (ECT, China). The electrical resistivity ρ and Seebeck coefficient S were obtained simultaneously by the standard dc four-probe technique in an LSR-800 measurement system (Linseis, Germany). The thermal conductivity κ was calculated based on $\kappa=DC_pd$, where D is the thermal diffusivity measured in vacuum using the laser flash technique on an LFA1000 system (Linseis, Germany), C_p is the specific heat capacity measured using a differential scanning calorimeter (Netzsch DSC200F3), and d is the bulk density of the prepared samples determined by the dimensions and mass of the samples and then reconfirmed by the Archimedes method. The porosity ε was calculated *via* $\varepsilon= 1-d/d_0$, where d is the experimental density and d_0 is the theoretical density of CdO which is calculated to be 8.27 g/cm^3. The uncertainty in the Seebeck coefficient and electrical conductivity measurements is within 5%, and the uncertainty of the thermal conductivity is estimated to be about 9%, considering the uncertainties for D, C_p and d. The combined uncertainty for ZT calculation is about 15%.

3. Results and discussion

Fig.1(a) shows the XRD θ-2θ scans of the $Cd_{1-x-y}Mg_xCa_yO$ ceramic samples. All the diffraction peaks of these Mg/Ca substituted samples can be indexed to the cubic CdO with space group $Fm\bar{3}m$ (225), and no other phase is observed within the detection limit of XRD. We calculate the lattice parameters of these samples according to the positions of the XRD peaks, which are presented in Fig.1(b).

Here the dashed lines are the calculated lattice parameters of $Cd_{1-x}Mg_xO$ and $Cd_{1-y}Ca_yO$ alloys based on the Vegard's law. As the ionic radii of Cd^{2+}(0.97 Å) is larger than that of Mg^{2+} (0.66 Å) while smaller than that of Ca^{2+} (0.99 Å), the lattice parameters of the Mg/Ca substituted samples fluctuate with different Mg/Ca concentrations, and the values are scattered in between the calculated lattice parameters of $Cd_{1-x}Mg_xO$ and $Cd_{1-y}Ca_yO$.

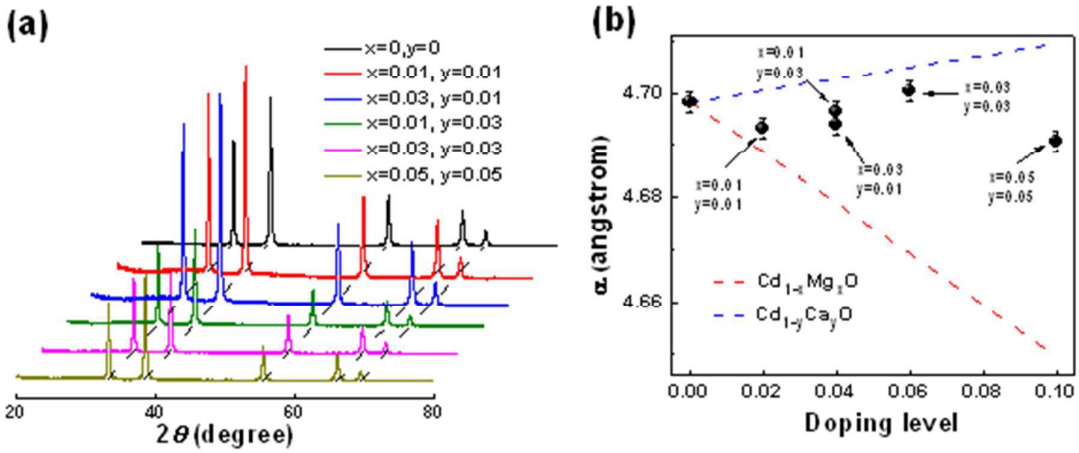

Fig.1 XRD patterns and lattice parameters of the $Cd_{1-x-y}Mg_xCa_yO$ ($0 \le x, y \le 0.05$) ceramic samples. (a) XRD patterns of the samples and (b) lattice parameters as a function of doping concentration, the dashed lines are the calculated lattice parameters of $Cd_{1-x}Mg_xO$ and $Cd_{1-y}Ca_yO$ alloys based on the Vegard's law.

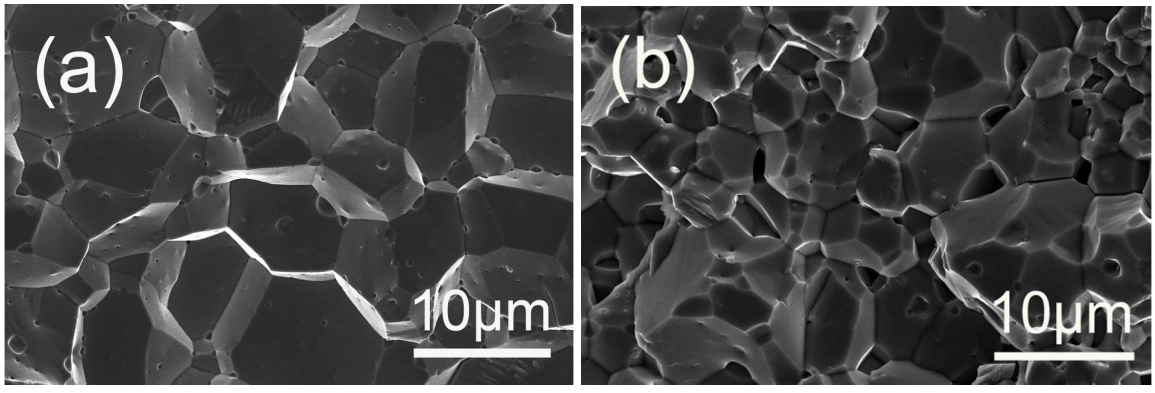

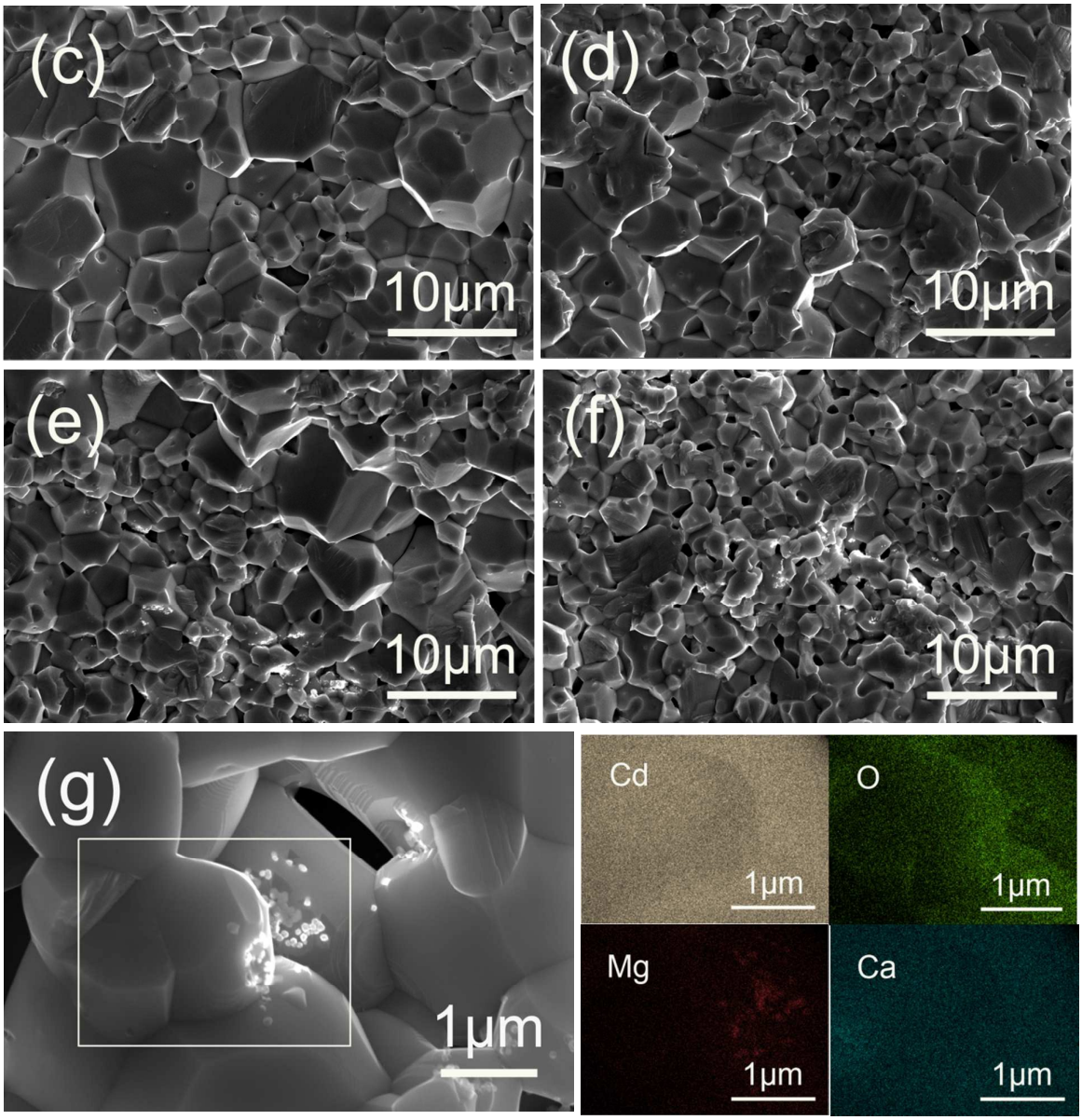

Fig.2 The fractured cross-sectional SEM micrographs and element mappings of (a) CdO; (b) $Cd_{0.98}Mg_{0.01}Ca_{0.01}O$; (c) $Cd_{0.96}Mg_{0.03}Ca_{0.01}O$; (d) $Cd_{0.96}Mg_{0.01}Ca_{0.03}O$ (e) $Cd_{0.94}Mg_{0.03}Ca_{0.03}O$; (f) $Cd_{0.90}Mg_{0.05}Ca_{0.05}O$, (g) is the magnified SEM and element mappings of $Cd_{0.90}Mg_{0.05}Ca_{0.05}O$.

Fig.2 shows the fractured cross-sectional SEM images of the $Cd_{1-x-y}Mg_xCa_yO$ ceramics, from which a significant grain refinement effect can be observed in the Mg and Ca substituted samples. Pristine CdO ceramic sample exhibits morphology of closely packed particles with diameters of ~10 μm (Fig. 2(a)), while the introduction

of Mg and Ca leads to the presence of some small grains with diameters of ~2 μm (Fig.2(b)-(f)). These small grains are clustered non-uniformly among the large particles and increase obviously with the substituting concentration, giving rise to an increment in grain boundaries. For $Cd_{0.90}Mg_{0.05}Ca_{0.05}O$, these small grains become dominant and the average grain size decreases drastically when compared with the pristine CdO. The decrease in grain size mainly originates from the pinning effect of the Mg/Ca that locate in or near the grain boundary regions, these additives can inhibit the movement of grain boundaries and prevent the grains from further growth [22-24], similar grain refinement effect is also observed in other oxides [25, 26]. It is noteworthy that some fine white crystallites can be detected besides the small grains. To better observe these fine crystallites, a magnified SEM image of the $Cd_{0.90}Mg_{0.05}Ca_{0.05}O$ sample is provided in Fig.2(g). As can be seen from Fig.2(g), these crystallites are some nano-sized precipitates. The EDX elemental mapping results show that, Cd, Ca and O elements distribute uniformly in the $Cd_{0.90}Mg_{0.05}Ca_{0.05}O$, whereas for Mg, some high content areas (brighter red) can be detected corresponding to the clustered precipitates, suggesting that the nano-sized precipitates are Mg-riched phases. In addition, some pores are also presented in the $Cd_{1-x-y}Mg_xCa_yO$ samples and increase gradually with the substituting concentration, hence the porosity of the samples experiences an evident increment from 1.3% for the pristine CdO to 18.1% for the $Cd_{0.90}Mg_{0.05}Ca_{0.05}O$ (Table 1), indicating a possible reduction of thermal conductivity in the heavily substituted samples [27, 28].

Table 1 Porosity ε, room temperature carrier concentration n and mobility μ of the $Cd_{1-x-y}Mg_xCa_yO$ ceramic samples.

Sample	Porosity	Carrier concentration(cm^{-3})	Mobility($cm^2\ V^{-1}\ s^{-1}$)
CdO	1.3%	4.1×10^{19}	125
$Cd_{0.98}Mg_{0.01}Ca_{0.01}O$	5.8%	3.6×10^{19}	109
$Cd_{0.96}Mg_{0.03}Ca_{0.01}O$	6.4%	3.0×10^{19}	111
$Cd_{0.96}Mg_{0.01}Ca_{0.03}O$	10.3%	2.9×10^{19}	102
$Cd_{0.94}Mg_{0.03}Ca_{0.03}O$	15.0%	2.7×10^{19}	93
$Cd_{0.90}Mg_{0.05}Ca_{0.05}O$	18.1%	8.5×10^{18}	161

Table 1 lists the room temperature carrier concentration n and mobility μ of these $Cd_{1-x-y}Mg_xCa_yO$ samples. The carrier concentration decreases gradually with increasing Mg/Ca concentration in spite of the homovalence substitution of Mg^{2+} and Ca^{2+} for Cd^{2+}, from 4.1×10^{19} cm^{-3} for the pristine CdO to 8.5×10^{18} cm^{-3} for the $Cd_{0.90}Mg_{0.05}Ca_{0.05}O$. The reduction in carrier concentration is suggested to be mainly caused by the change of CdO band structure after introducing other materials that have different electron affinities [29, 30]. When introducing Mg and Ca into the CdO matrix, the conduction band minimum (CBM) of the CdO will shift upward due to the large difference in the electron affinities of CdO and MgO/CaO [31], thus the energy level of the donor impurities in CdO becomes relatively deeper due to the upward movement of the CBM. This change in band structure will result in reduced ionization of oxygen vacancies or cadmium interstitials, and finally a decrease in carrier concentration. In addition, the increased grain boundaries and disorders in the substituted samples could cause the localization of the carriers, which can also result

in the decrease of carrier concentration. As for the carrier mobility μ of the samples, it decreases from 125 cm^2 V^{-1} s^{-1} to 93 cm^2 V^{-1} s^{-1} when the Mg/Ca concentration increases up to 3%, which can be attributed to the enhanced scatterings at grain boundaries and disorders induced by the substitution. However, further addition of Mg and Ca (i.e., sample of $Cd_{0.90}Mg_{0.05}Ca_{0.05}O$) leads to an abnormal increase in μ. This increment possibly arises from the decreased ionized impurity scatterings since the carrier concentration of this sample decreases to the order of 10^{18} cm^{-3}.

Fig.3(a)-(c) are the temperature dependences of electrical resistivity ρ, Seebeck coefficient S and power factor S^2/ρ of the $Cd_{1-x-y}Mg_xCa_yO$ samples. As can be seen from Fig.3(a), each sample shows an increasing trend with the increase of temperature, indicating a metal-like conducting behavior. The slight decrease in ρ for the 5% Mg/Ca substituted sample mostly results from the contribution of thermal activated carriers. As the substituting concentration increases, the electrical resistivity ρ of the samples increases gradually, this increment is mainly caused by the decreased carrier concentration. Fig.3(b) represents the variation of Seebeck coefficient S of the $Cd_{1-x-y}Mg_xCa_yO$ samples as a function of temperature. The absolute Seebeck coefficient $|S|$ of each sample increases monotonically with temperature, and the negative values of S demonstrate that all these samples are n-type conducting. Moreover, the value of $|S|$ increases with the substituting concentration owing to the decrease of carrier concentration. Although increment in $|S|$ is achieved *via* Mg/Ca substituting, deteriorated electrical resistivity is also observed in the substituted samples, consequently, the S^2/ρ values of the substituted samples are still lower than

that of the pristine CdO, as can be seen in Fig.3(c).

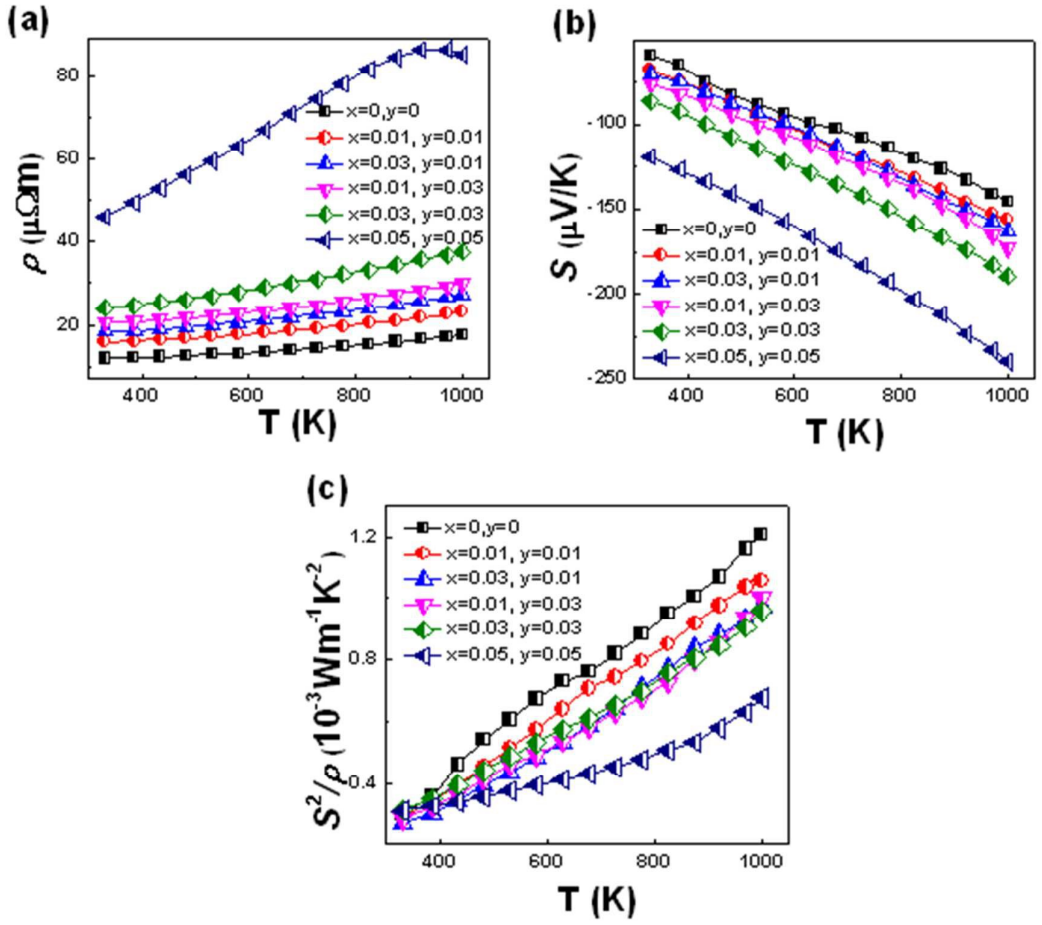

Fig.3 Temperature dependence of (a) Seebeck coefficient S, (b) electrical resistivity ρ and (c) power factor S^2/ρ of the $Cd_{1-x-y}Mg_xCa_yO$ ($0 \le x, y \le 0.05$) ceramics.

The microstructure and electrical property of the CdO ceramic samples all experienced obvious changes by incorporating Mg and Ca, which will have significant effects on the thermal transport properties of the samples. Fig.4(a) presents the thermal conductivity κ of these $Cd_{1-x-y}Mg_xCa_yO$ samples at different temperatures. It clearly shows that the value of κ decreases with increasing Mg/Ca concentration over the whole measured temperature. At about room temperature, the κ value of $Cd_{0.90}Mg_{0.05}Ca_{0.05}O$ drops quickly to 3.5 W/mK, 55% lower than that of

the undoped CdO, and further decreases to 1.7 W/mK when the temperature reaches about 1000 K. This reduction in κ suggests the Mg/Ca substituting strategy is very effective in suppressing the thermal conductivity of CdO ceramics. To better evaluate the effects of Mg/Ca substituting on the thermal transport of carriers (κ_c) and phonons (κ_{ph}) of the samples, we calculate the contribution of these two parts to the total thermal conductivity κ. Fig.4(b) plots the temperature dependence of κ_c of the different samples, here κ_c is related to the electrical resistivity ρ through the Wiedemann–Franz law $\kappa_c = LT/\rho$ (where L is the Lorenze factor derived from $L = 1.5 + exp\left[-\frac{|S|}{116}\right]$ [32]). We can see from Fig.4(b) that, although κ_c experiences a detectable rise with increasing T, it contributes little to κ, and the introduction of Mg and Ca clearly decreases the carrier thermal conductivity due to the increased ρ.

The phonon thermal conductivity κ_{ph} of the samples is obtained by subtracting the electronic part from the total thermal conductivity, which is shown in Fig.4(c). Fig.4(c) clearly verifies that the heat is primarily carried by phonons in the $Cd_{1-x-y}Mg_xCa_yO$ system, and the Mg/Ca substitution can greatly decrease the phonon thermal conductivity κ_{ph}. For example, at ~1000 K, the κ_{ph} values decrease drastically from 2.57 W/mK for the pristine CdO to 1.53 W/mK for the $Cd_{0.90}Mg_{0.05}Ca_{0.05}O$, which is close to the calculated amorphous limit for thermal conductivity κ_{min} of CdO [21]. Multiple reasons are proposed to be responsible for the reduction of κ_{ph}. Firstly, due to the distinct differences in mass, size and interatomic coupling force between Cd and Mg/Ca atoms, the substituting of Mg/Ca on Cd site will distort the CdO lattices. The defects caused by the distortions of crystal lattices may lead to strong

phonon scatterings that decrease the phonon thermal conductivity of the samples. Secondly, the increased grain boundaries and pores induced by Mg/Ca substitution can enhance the phonon scatterings and thus further suppress κ_{ph}. Thirdly, the nanoscale Mg-riched precipitants appeared in the Mg/Ca heavily substituted samples, as seen in the aforementioned SEM images, also can serve as phonon scattering sources to decrease the phonon thermal conductivity.

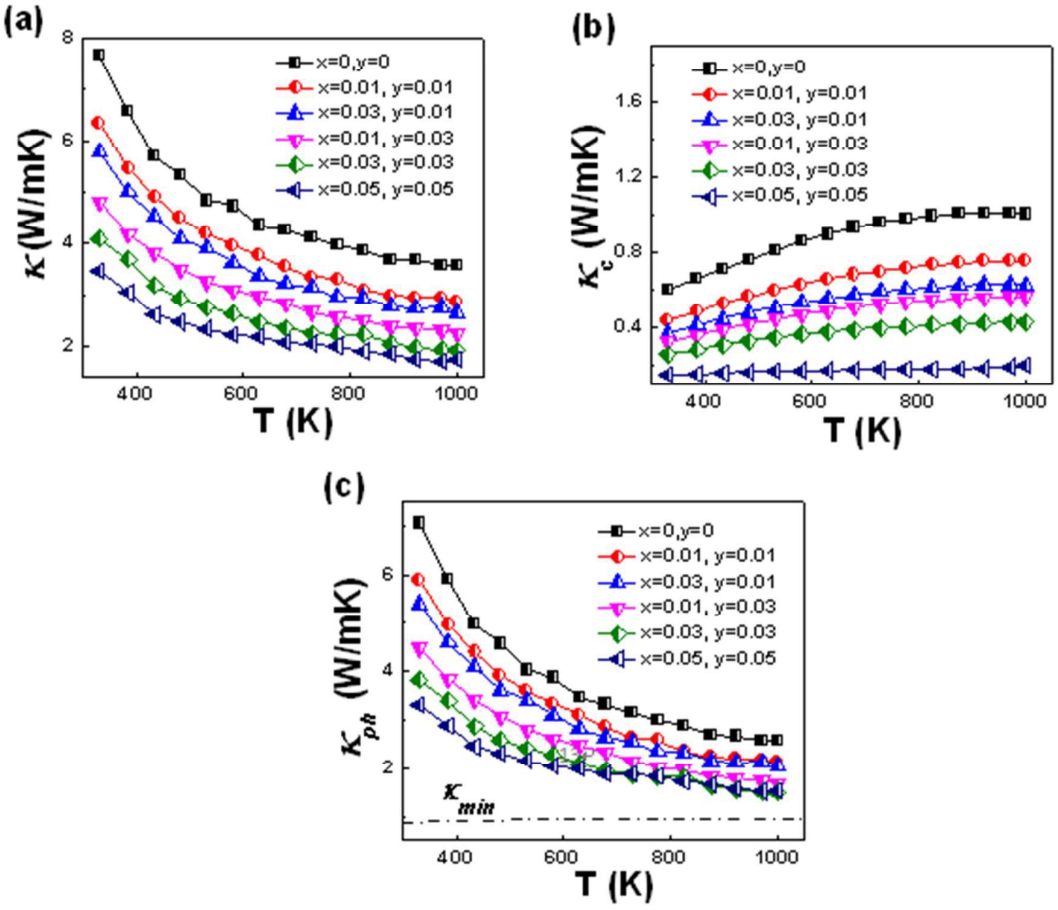

Fig. 4 The temperature dependence of (a) total thermal conductivity κ, (b) carrier thermal conductivity κ_c and (c) phonon thermal conductivity κ_{ph} of the $Cd_{1-x-y}Mg_xCa_yO$ ($0 \le x, y \le 0.05$) ceramic samples. The dash line is the calculated κ_{min} of CdO from literature 21.

The *ZT* values of these $Cd_{1-x-y}Mg_xCa_yO$ ceramic samples as a function of temperature are displayed in Fig.5. Although the power factor experiences detectable

decrease after introducing Mg and Ca, when the thermal conductivity is taken into account, it is obvious that all the substituted samples show higher *ZT* values than the pure one. The optimum substituted sample of $Cd_{0.94}Mg_{0.03}Ca_{0.03}O$ reaches the most substantial improvement in *ZT* with a maximum value of 0.5 at ~1000 K, 56% higher than the pristine CdO, also higher than $Cd_{0.97}Mg_{0.03}O$ (*ZT*~0.34) and $Cd_{0.97}Ca_{0.03}O$ (*ZT*~0.44) ceramics. As far as we know, this is the highest value reported so far in the n-type oxide thermoelectric materials, proving that suppressing the thermal conductivity *via* Mg/Ca substitution is a promising way to boost the TE efficiency of CdO ceramics.

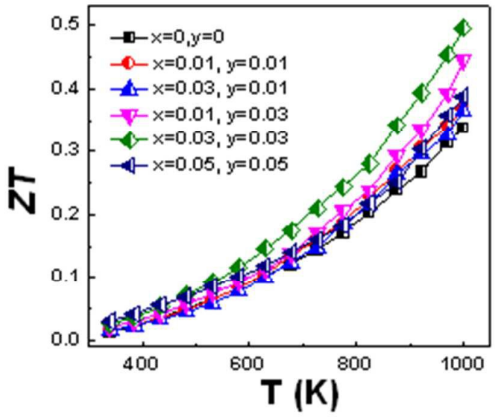

Fig.5 Temperature dependence of *ZT* for $Cd_{1-x-y}Mg_xCa_yO$ ($0 \le x, y \le 0.05$) samples.

4. Conclusion

In this paper, we reported enhanced thermoelectric performance of CdO ceramics by Mg/Ca substitution. Although Mg/Ca substitution had a negative effect on the power factor of the CdO ceramics due to the increased electrical resistivity, it can suppress the thermal conductivity κ owing to the significant enhanced phonon scatterings by defects, grain boundaries, micro-pores and Mg-riched nanoprecipitates

in the substituted samples. Benefiting from the low κ value, a ZT of 0.5 at ~1000 K was achieved for the optimum sample of $Cd_{0.94}Mg_{0.03}Ca_{0.03}O$. This is the highest value reported in the CdO-based thermoelectric materials, and further optimization is still expected in this system.

Acknowledgment:

This project was supported by the National Natural Science Foundation of China (No. 51372064 and No. 51401186), the Nature Science Foundation of Hebei Province, China (No. 2013201249 and No. A2014201176) and the Fostering Foundation for the Distinguished Ph.D. Dissertation of Hebei University.

Reference

1 L. D. Zhao, S. H. Lo, Y. Zhang, H. Sun, G. Tan, C. Uher, C. Wolverton, V. P. Dravid and M. G. Kanatzidis, *Nature*, 2014, **508**, 373-377.

2 K. Biswas, J. He, I. D. Blum, C. I. Wu, T. P. Hogan, D. N. Seidman, V. P. Dravid and M. G. Kanatzidis, *Nature*, 2012, **489**, 414-418.

3 J. P. Heremans, V. Jovovic, E. S. Toberer, A. Saramat, K. Kurosaki, A. Charoenphakdee, S. Yamanaka and G. J. Snyder, *Science*, 2008, **321**, 554-557.

4 K. Park, K.Y. Ko, W.-S. Seo, *J. Eur. Ceram. Soc.*, 2005, **25**, 2219-2222.

5 X. Zhao, H. Wang, S. Wang, D. Elhadj, J. Wang and G. Fu, *RSC Adv.*, 2014, **4**, 57148-57152.

6 F. Kahraman, M.A. Madre, Sh. Rasekh, C. Salvador, P. Bosque, M.A. Torres, J.C. Diez and A. Sotelo, *J. Eur. Ceram. Soc.*, 2015, **35**, 3835-3841.

7 I. Terasaki, Y. Sasago and K. Uchinokura, *Phys. Rev. B: Condensed Matter*, 1997, **56**, R12685-R612687

8 N. Van Nong, N. Pryds, S. Linderoth and M. Ohtaki, *Adv. Mater.*, 2011, **23**, 2484-2490.

9 R. Funahashi and M. Shikano, *Appl. Phys. Lett.*, 2002, **81**, 1459-1461.

10 N. Wang, H. Chen, H. He, W. Norimatsu, M. Kusunoki and K. Koumoto, *Sci. rep.*, 2013, **3**, 3449.

11 L. Bocher, M. H. Aguirre, D. Logvinovich, A. Shkabko, R. Robert, M. Trottmann and A. Weidenkaff, *Inorg. Chem.*, 2008, **47**, 8077-8085.

12 A. Z. Barasheed, S. R. S. Kumar and H. N. Alshareef, *J. Mater. Chem. C*, 2013, **1**, 4122-4127.

13 E. Combe, E. Guilmeau, E. Savary, S. Marinel, R. Cloots, R. Funahashi and F. Boschini, *J. Eur. Ceram. Soc.*, 2015, **35**, 145-151.

14 A. V. Kovalevsky, A. A. Yaremchenko, S. Populoh, P. Thiel, D. P. Fagg, A. Weidenkaff and J. R. Frade, *Phys. Chem. Chem. Phys.*, 2014, **16**, 26946-26954.

15 Y.-H. Zhu, W.-B. Su, J. Liu, Y.-C. Zhou, J. Li, X. Zhang, Y. Du and C.-L. Wang, *Ceram. Int.*, 2015, **41**, 1535-1539.

16 J. L. Lan, Y. Liu, Y. H. Lin, C.W. Nan, Q. Cai and X. Yang, *Sci. rep*., 2015, **5**, 7783.

17 M. Ohtaki, K. Araki and K. Yamamoto, *J. Electron. Mater.*, 2009, **38**, 1234-1238.

18 S. Wang, F. Liu, Q. Lü, S. Dai, J. Wang, W. Yu and G. Fu, *J. Eur. Ceram. Soc.*, 2013, **33**, 1763-1768.

19 L. Li, S Liang, S. Li, J. Wang, S. Wang, G. Dong and G. Fu, *Nanotechnology*, 2014, **25**, 425402.

20 L. Lindsay and D. S. Parker, *Phys. Rev. B*, 2015, **92**, 144301.

21 L. Gao, S. Wang, R. Liu, S. Zhai, H. Zhang, J. Wang and G. Fu, *J. Alloy. Compd.*, 2016, **662**, 213-219.

22 M. K. Cinibulk, *J. Am. Ceram. Soc.*, 2004, **87**, 692-695.

23 S. S. Lo, D. Huang, C. H. Tu, C.-H. Hou and C.-C. Chen, *J. Phys. D: Appl. Phys.*, 2009, **42**, 095420.

24 F. F. Lange and M. M. Hirlinger, *J. Am. Ceram. Soc.*, 1984, **67**, 164-168.

25 K. Park, J. K. Seong and G. H. Kim, *J. Alloy. Compd.*, 2009, **473**, 423-427.

26 P. Jood, R. J. Mehta, Y. Zhang, G. Peleckis, X. Wang, R. W. Siegel, T. Borca-Tasciuc, S. X. Dou and G. Ramanath, *Nano Lett.*, 2011, **11**, 4337-4342.

27 F. R. Charvat and W. D. Kingery, *J. Am. Ceram. Soc.*, 1957, **40**, 306-315.

28 Z. Wang, J. E. Alaniz, W. Jang, J. E. Garay and C. Dames, *Nano Lett.*, 2011, **11**, 2206-2213.

29 G. Chen, K. M. Yu, L. A. Reichertz and W. Walukiewicz, *Appl. Phys. Lett.*, 2013, **103**, 041902.

30 C. A. Francis, D. M. Detert, G. Chen, O. D. Dubon, K. M. Yu and W. Walukiewicz, *Appl. Phys. Lett.*, 2015, **106**, 022110.

31 G. Murtaza, B. Amin, S. Arif, M. Maqbool, I. Ahmad, A. Afaq, S. Nazir, M. Imran and M. Haneef, *Comp. Mater. Sci.*, 2012, **58**, 71-76

32 H.-S. Kim, Z. M. Gibbs, Y. Tang, H. Wang and G. J. Snyder, *APL Materials*, 2015, **3**, 041506.

A high *ZT* of 0.5 at about 1000 K has been achieved in the $Cd_{0.94}Mg_{0.03}Ca_{0.03}O$, which is the highest *ZT* ever reported among the n-type oxides in this temperature range.